ChemComm

COMMUNICATION

View Article Online
View Journal

Cite this: DOI: 10.1039/d1cc05977g

Received 23rd October 2021,
Accepted 7th December 2021

DOI: 10.1039/d1cc05977g

rsc.li/chemcomm

A self-assembled subphthalocyanine-based nanophotosensitiser for photodynamic therapy†

Nicolás M. Casellas,‡[ab] Gaole Dai,‡[c] Evelyn Y. Xue,[c] Alba Fonseca,[a] Dennis K. P. Ng,*[c] Miguel García-Iglesias*[abd] and Tomás Torres*[ab]

A subphthalocyanine substituted with nine tetra(ethylene glycol) chains on the periphery has been synthesised. This novel amphiphilic and cone-shaped compound can self-assemble in water into spherical nanoparticles with a hydrodynamic diameter of 154 nm. These nanoparticles can be taken up readily by cancer cells and localised predominately in lysosomes where they disassemble gradually, leading to activation in fluorescence emission and, photocytotoxicity, showing IC_{50} values of as low as 1.2 μM.

Photodynamic therapy (PDT) is a clinically approved treatment modality for a range of cancers. It utilises a non-toxic photosensitiser (PS) that in combination with selective light irradiation and tissue oxygen triggers the generation of reactive oxygen species (ROS), capable of destroying malignant cells.[1] However, the use of traditional molecular PSs has inherent drawbacks that hamper the full development of PDT, as the combination of poor transport, low tumour selectivity and the "always-on" property generally leads to post-treatment risks associated with harmful photosensitisation.[2] In recent decades, a great deal of research has been carried out to improve the loading and transport of PSs, which play a critical role in the overall efficacy of PDT.[3] In this context, hierarchically organised supramolecular assemblies based on different monomeric PSs represent an ideal platform to improve some of the deficiencies mentioned above.[4] In such adaptable assemblies, monomeric PS structures can be customised, which opens the possibility of rationally designing nanostructured supramolecular nanoparticles with different sizes and morphologies, and thus for controlling their transport and internalisation properties.[5] Furthermore, the self-assembly of PSs may form nanostructured materials that undergo disassembly and reconstruction as a result of the relatively weak intermolecular interactions between the monomers. Therefore, the inherent reversibility of the supramolecular assemblies can be further utilised to precisely control the ROS generation *via* contact- or self-quenching of the PSs in order to minimise the photosensitisation side effects caused by the "always-on" PSs.[6]

Subphthalocyanines (SubPcs)[7] represent a promising class of PSs. They exhibit high fluorescence and singlet oxygen quantum yields that in combination with their intense absorption and emission near the therapeutic optical window make them highly suitable, although scarcely studied, PSs for PDT.[8] In fact, very recently, it has been observed that properly substituted SubPcs can display high photocytotoxicities in nanomolar concentrations.[9] Moreover, SubPcs represent a very interesting building block for self-assembled nanosystems as their unusual cone-shaped structure allows for head-to-tail stacking of the monomeric units endowed with a very small axial ligand.[10] In this regard, by merging for the first time both, the excellent photosensitizing properties of SubPcs and their self-assembling capacity, we report herein the synthesis of a rationally designed SubPc-based amphiphilic PS, capable of self-assembling into well-defined single-component supramolecular nanoparticles in aqueous media displaying activatable photoactivity.

Fig. 1a shows the structure of the monomeric unit **SubPc(PEG)$_3$** designed and synthesised for the generation of water-soluble supramolecular aggregates (see ESI† for the synthetic procedure and characterisation). The self-assembling monomer has a C_3 symmetry, and the SubPc-F bowl-shaped core provides the robustness and directionality to the supramolecular aggregates. Moreover, as previously observed, the presence of a strongly polar axial B–F bond might reinforce the head-to-tail association due to the dipole–dipole interactions.[10] Finally, the compound also contains nine tetra(ethylene glycol) side-chains introduced to the SubPc periphery in order to

[a] *Department of Organic Chemistry and Institute for Advanced Research in Chemical Sciences (IadChem), Universidad Autónoma de Madrid, Calle Francisco Tomás y Valiente, 7, Madrid 28049, Spain. E-mail: tomas.torres@uam.es*
[b] *IMDEA Nanociencia, c/Faraday 9, Cantoblanco, Madrid 28049, Spain*
[c] *Department of Chemistry, The Chinese University of Hong Kong, Shatin, N. T., Hong Kong, China. E-mail: dkpn@cuhk.edu.hk*
[d] *QUIPRE Department, University of Cantabria, Avd. de Los Castros, 46, Santander 39005, Spain. E-mail: giglesiasm@unican.es*

† Electronic supplementary information (ESI) available. See DOI: 10.1039/d1cc05977g

‡ These authors have contributed equally.

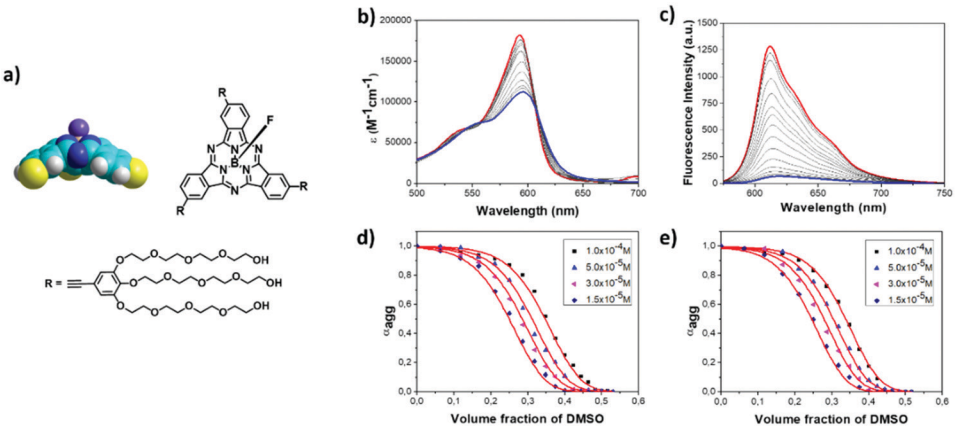

Fig. 1 (a) Molecular structure of **SubPc(PEG)$_3$** and schematic representation of the SubPc bowl-shaped core. Titration of an aqueous solution of **SubPc(PEG)$_3$** (blue) until reaching the disaggregated state in DMSO (red) at a constant concentration of 5.0 × 10^{-5} M recorded by (b) UV-vis and (c) fluorescence (λ_{ex} = 520 nm) spectroscopy at 298 K. Polymerization curves obtained after denaturation of the aggregates in water by increasing the volume fraction of DMSO to four different concentrations determined by (d) UV-vis and (e) fluorescence spectroscopy of **SubPc(PEG)$_3$** at 298 K fitted with the SD model[12] (red lines). In order to reach the monomeric state, it was necessary to add up to 45% of DMSO. The emission spectra had been previously normalised due to the fluorescence auto-deactivation phenomena between the chromophores.

increase the water solubility and enhance the permeability and retention effect.[11]

The spectroscopic features of **SubPc(PEG)$_3$** were analysed in water and dimethylsulfoxide (DMSO), respectively, using UV-vis and fluorescence spectroscopic methods (Fig. S1, ESI,† and Fig. 1b and c). The Q-band of **SubPc(PEG)$_3$** in water (at 598 nm) was significantly less intense and slightly red-shifted with respect to that in DMSO (at 590 nm) (Fig. 1b). A similar shift has been previously reported for the head-to-tail aggregates of the dodecyloxy analogue of **SubPc(PEG)$_3$**,[10b] indicating the formation of aggregates in water. In the respective fluorescence spectra, a very weak emission band was observed in water at 620 nm. In contrast, the band was much stronger and slightly blue-shifted to 612 nm in DMSO (Fig. 1c). Therefore, both spectroscopic techniques pointed out to the formation of head-to-tail assemblies of **SubPc(PEG)$_3$** in water, resulting in a strongly quenched photoactivity.

The size and morphology of the **SubPc(PEG)$_3$** aggregates in water were examined by transmission electron microscopy (TEM), showing that they were spherical in shape with a diameter of 136 ± 11 nm (Fig. 2a). The dynamic light scattering (DLS) method was also used to measure the hydrodynamic diameter of the nanoparticles. The results showed that the size distribution was unimodal with a hydrodynamic diameter of 154 ± 4 nm (Fig. 2b). The small polydispersity index (PDI) (0.15 ± 0.04) indicated that these nanoparticles were well dispersed in water without significant aggregation.

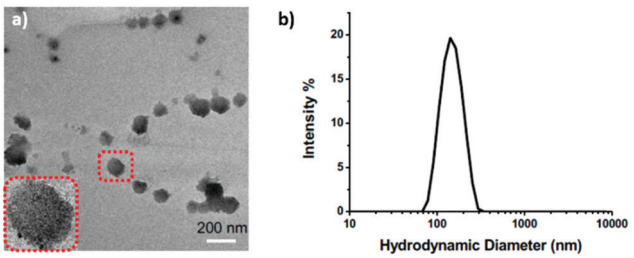

Fig. 2 (a) TEM image of **SubPc(PEG)$_3$** nanoparticles (with 100 μM SubPc) in water. (b) Hydrodynamic diameter distribution of **SubPc(PEG)$_3$** nanoparticles in water measured by DLS.

The thermodynamic aspects governing the self-assembly of **SubPc(PEG)$_3$** were studied by gradually increasing the volume fraction of a "good solvent" such as DMSO (Fig. 1b and c), since the supramolecular aggregates showed a critical aggregation concentration (CAC) above 10^{-7} M together with high thermostability (Fig. S2, ESI†).

The appearance of isosbestic points during the titrations in the UV-vis spectra suggested the presence of an equilibrium between the monomeric and aggregated species. By plotting the degree of aggregation as a function of the volume fraction of DMSO, sigmoidal curves were obtained as shown in Fig. 1d and e, indicating an isodesmic aggregation process.[12] The analysis of the data following a solvent-denaturation SD model[13] reveals a ΔG value of −43.0 kJ mol^{-1} in water and a degree of cooperativity (σ) of unity, with excellent correlation, which confirm an equal-K aggregation mechanism (see the experimental details and other thermodynamic parameters in Table S1, ESI†).

The photosensitising property of **SubPc(PEG)$_3$** was evaluated in DMSO and D_2O, respectively. Singlet oxygen quantum yields (Φ_Δ) were determined in both solvents using a relative method[14] employing the chemical scavenger 1,3-diphenylisobenzofuran (DPBF) (in DMSO) or 9,10-anthracenediyl-bis(methylene)dimalonic acid (ABDA) (in D_2O) (see the experimental procedure and Fig. S3 in ESI†). Under these conditions, a dramatic difference in the Φ_Δ value was found. Whilst the monomeric form of **SubPc(PEG)$_3$** in DMSO could generate $^1O_2$ effectively (Φ_Δ = 0.54), the $^1O_2$ production efficiency of **SubPc(PEG)$_3$** nanoparticles in D_2O was much lower (Φ_Δ = 0.11). Moreover, when using ABDA, a specific scavenger for $^1O_2$,[15] in DMSO, **SubPc(PEG)$_3$** was more efficient in sensitising the

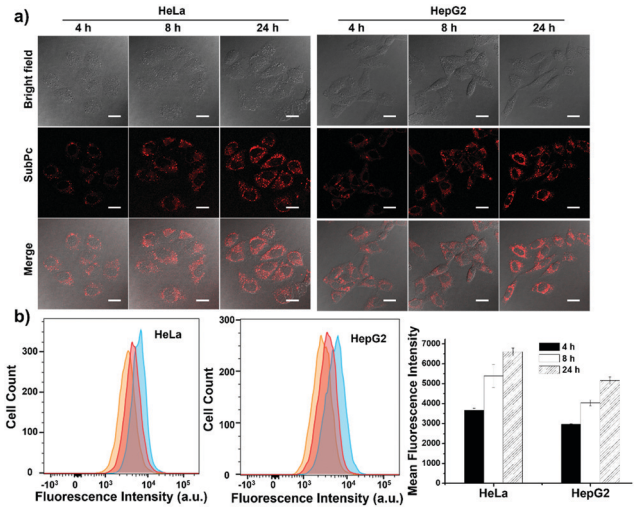

Fig. 3 (a) Bright-field, fluorescence and merged images of HeLa and HepG2 cells after incubation with **SubPc(PEG)$_3$** nanoparticles (with 5 μM SubPc) for 4, 8 or 24 h. Scale bar: 25 μm. (b) Flow cytometric measurements for the two cell lines after the above treatments. Data are presented as the mean ± standard deviation (SD) of three independent experiments.

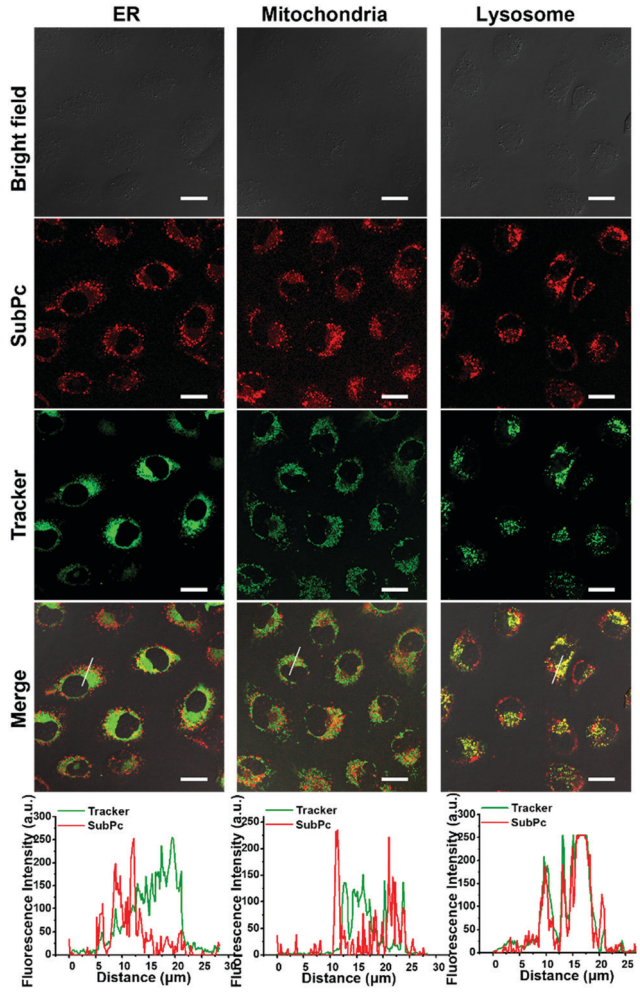

Fig. 4 Visualisation of the intracellular fluorescence of **SubPc(PEG)$_3$** nanoparticles (after incubation for 24 h) and various subcellular trackers in HeLa cells. The corresponding bright-field and merged images are given in rows 1 and 4, respectively. The figures on the bottom show the fluorescence intensity profiles of **SubPc(PEG)$_3$** nanoparticles and the different trackers traced along the lines in the corresponding images in row 4. Scale bar: 25 μm.

photo-decay of this probe, suggesting that the photosensitisation proceeded through a type II mechanism.[16]

The cellular uptake of **SubPc(PEG)$_3$** nanoparticles was then examined using human cervical carcinoma HeLa cells and human hepatocellular carcinoma HepG2 cells. All the cells were incubated with **SubPc(PEG)$_3$** nanoparticles (with 5 μM SubPc) for 4, 8 or 24 h. At this concentration in the culture medium, **SubPc(PEG)$_3$** was found to be in a nanoparticle form with a hydrodynamic diameter of 179 ± 6 nm (Fig. S4, ESI†). As shown in Fig. 3a, the intracellular fluorescence due to the SubPc remained weak after incubation for 4 h, but the intensity increased when the incubation was prolonged to 8 and 24 h. As the SubPc molecules were aggregated and quenched inside the nanoparticles, the increase in fluorescence intensity suggested that the nanoparticles were disassembled gradually inside the cells over a period of 24 h, releasing free SubPc molecules in the cytoplasm. Fig. 3b shows the quantified fluorescence intensities determined by flow cytometry under these conditions. It can be seen that the intracellular fluorescence intensity increased gradually for both the cell lines over 24 h. The results were in good agreement with those obtained by confocal fluorescence microscopy.

Moreover, we monitored the stability of **SubPc(PEG)$_3$** nanoparticles in the culture medium, where the size and zeta potential of the nanoparticles remained unchanged, and the fluorescence persisted fully quenched over a period of 24 h (Fig. S5, ESI†). Therefore, these results clearly indicated that the nanoparticles were disassembled inside the cells.

The subcellular localisation of **SubPc(PEG)$_3$** nanoparticles was further examined with confocal fluorescence microscopy. After incubation with **SubPc(PEG)$_3$** nanoparticles (with 5 μM SubPc) for 24 h, the HeLa and HepG2 cells were stained with LysoTracker Green DND-26 (2 μM), Mito-Tracker Green FM (0.2 μM) or ER-Tracker Green (1 μM) for 30 min, 15 min or 15 min, respectively, before being examined with a confocal laser scanning microscope. As shown in Fig. 4 (for HeLa cells) and Fig. S6 (ESI†) (for HepG2 cells), the fluorescence image and intensity profile for **SubPc(PEG)$_3$** nanoparticles could overlap well with those for LysoTracker, but not for the other two trackers inside the cells. Pearson's correlation coefficient (PCC) was significantly higher for lysosomes, suggesting that **SubPc(PEG)$_3$** nanoparticles tended to reside in the lysosomes (Fig. S7, ESI†).

To gain a better understanding about the intracellular trafficking and the disassembling process of the nanoparticles, we also studied their subcellular localization after incubation for a shorter period of time. It was found that after 4 h, the fluorescence was also localized in the lysosomes of HeLa cells (Fig. S8 and S9, ESI†) suggesting an internalization *via* endocytosis.[17] Therefore, they are likely trafficked to the early

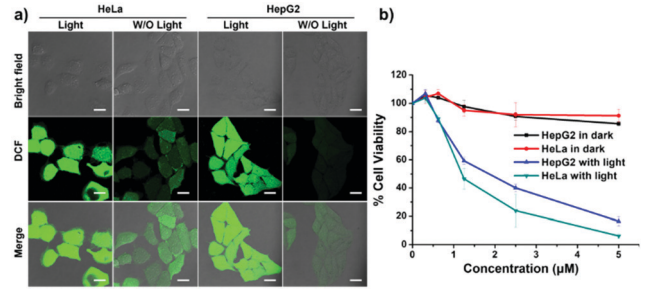

Fig. 5 (a) Intracellular ROS production as reflected by the intracellular fluorescence of DCF in HeLa and HepG2 cells after being treated with **SubPc(PEG)$_3$** nanoparticles with or without irradiation (λ > 515 nm, 25.5 mW cm^{-2}, and 30.6 J cm^{-2}). Scale bar: 25 μm. (b) Cell viability of HeLa and HepG2 cells upon treatment with **SubPc(PEG)$_3$** nanoparticles with or without irradiation (λ > 515 nm, 25.5 mW cm^{-2}, and 30.6 J cm^{-2}). Data are presented as the mean ± standard error of the mean of three independent experiments, each performed in quadruplicate.

endosomes and then the late endosomes, and eventually to the lysosomes where degradative enzymes[18] may trigger the disassembly of the nanoparticles.[19]

The ability of **SubPc(PEG)$_3$** nanoparticles to generate ROS inside cancer cells was also examined using 2′,7′-dichlorodihydrofluorescein diacetate (DCFDA) as the probe, which undergoes deacetylation rapidly in the presence of ROS inside the cells, changing from a non-fluorescent chemically reduced form of fluorescein into the highly fluorescent 2′,7′-dichlorofluorescein (DCF).[20] In this study, All the cells were first treated with **SubPc(PEG)$_3$** nanoparticles (with 5 μM SubPc) for 24 h, followed by incubation with DCFDA for 30 min with or without irradiation (λ > 515 nm, 25.5 mW cm^{-2}, and 30.6 J cm^{-2}). The intracellular fluorescence remained very weak in the dark. In contrast, notable fluorescence due to DCF could be observed upon irradiation (Fig. 5a). The results indicated that the nanoparticles could serve as a photosensitiser and generate ROS inside the cells upon light irradiation.

The cytotoxicity of **SubPc(PEG)$_3$** nanoparticles against cancer cells was further determined by MTT assay [MTT = 3-(4,5-dimethylthiazol-2-yl)-2,5-diphenyltetrazolium bromide]. As shown in Fig. 5b, the dark cytotoxicity of **SubPc(PEG)$_3$** nanoparticles against HeLa and HepG2 cells was minimal at a SubPc concentration of up to 5 μM with over 85% of the cells remaining alive after the treatment. Upon irradiation (λ > 515 nm, 25.5 mW cm^{-2}, and 30.6 J cm^{-2}), the **SubPc(PEG)$_3$** nanoparticles exhibited significant photocytotoxicity. The IC$_{50}$ value, defined as the photosensitiser (SubPc) concentration required to kill 50% of the cells, was found to be 1.2 μM for HeLa cells and 1.9 μM for HepG2 cells, showing that the nanoparticles were highly photocytotoxic.

In conclusion, with a unique structural feature and amphiphilic character, **SubPc(PEG)$_3$** could assemble in aqueous media, forming a well-defined nanostructure. These nanoparticles could be internalised readily into cancer cells and localised in the lysosomes. Through gradual disassembling, the photosensitising nanosystem was activated, leading to cell death with IC$_{50}$ values of as low as 1.2 μM. The supramolecular approach presented here paves the way for the preparation of dynamic photosensitisers to precisely control the ROS generation *via* self-quenching, which can minimise the photosensitisation side effects caused by the ''always-on'' PSs during PDT treatments.

The financial support from MINECO (PID2020-116490GB-I00) is acknowledged. IMDEA Nanociencia acknowledges the support from the ''Severo Ochoa'' Programme (MINECO, Grant SEV2016-0686). M. G. I. thanks Santander Talent Attraction Research (STAR2) for financial support.

Conflicts of interest

There are no conflicts of interest to declare.

Notes and references

1 J. H. Correia, J. A. Rodrigues, S. Pimenta, T. Dong and Z. Yang, *Pharmaceutics*, 2021, **13**, 1332.
2 B. Rodríguez-Amigo, O. Planas, R. Bresolí-Obach, J. Torra, R. Ruiz-González and S. Nonell, in *Photodynamic Medicine: From Bench to Clinic*, ed. H. Kostron and T. Hasan, The Royal Society of Chemistry, 2016, pp. 23–62.
3 (*a*) Y. H. Bae, *J. Controlled Release*, 2009, **133**, 2–3; (*b*) J. J. Hu, Q. Lei and X. Z. Zhang, *Prog. Mater. Sci.*, 2020, **114**, 100685.
4 L. Zhao, Y. Xing, R. Wang, F. F. Yu and F. Yu, *ACS Appl. Bio Mater.*, 2020, **3**, 86–106.
5 I. Paramio, T. Torres and G. de la Torre, *ChemMedChem*, 2021, **16**, 2441–2451.
6 M. Yang, X. Li and J. Yoon, *Mater. Chem. Front.*, 2021, **5**, 1683–1693.
7 C. G. Claessens, D. Gonzalez-Rodríguez, S. M. Rodríguez-Morgade, A. Medina and T. Torres, *Chem. Rev.*, 2014, **114**, 2192–2277.
8 H. Xu, X.-J. Jiang, E. Y. M. Chan, W.-P. Fong and D. K. P. Ng, *Org. Biomol. Chem.*, 2007, **5**, 3987–3992.
9 J. Demuth, L. Gallego, M. Kozlikova, M. Machacek, R. Kucera, T. Torres, M. V. Martínez-Díaz and V. Novakova, *J. Med. Chem.*, 2021, **64**, 17436–17447.
10 A. V. Gorbunov, M. Garcia-Iglesias, J. Guilleme, T. D. Cornelissen, W. S. C. Roelofs, T. Torres, D. Gonzalez-Rodríguez, E. W. Meijer and M. Kemerink, *Sci. Adv.*, 2017, **3**, e1701017.
11 S. Mura and P. Couvreur, *Adv. Drug Delivery Rev.*, 2012, **64**, 1394–1416.
12 T. F. A. De Greef, M. M. J. Smulders, M. Wolffs, A. P. H. J. Schenning, R. P. Sijbesma and E. W. Meijer, *Chem. Rev.*, 2009, **109**, 5687–5754.
13 P. A. Korevaar, C. Schaefer, T. F. A. de Greef and E. W. Meijer, *J. Am. Chem. Soc.*, 2012, **134**, 13482–13491.
14 N. Nombona, K. Maduray, E. Antunes, A. Karsten and T. Nyokong, *J. Photochem. Photobiol., B*, 2012, **107**, 35–44.
15 T. Entradas, S. Waldron and M. Volk, *J. Photochem. Photobiol., B*, 2020, **204**, 111787.
16 X. Zhao, J. Liu, J. Fan, H. Chao and X. Peng, *Chem. Soc. Rev.*, 2021, **50**, 4185–4219.
17 (*a*) D. Manzanares and V. Ceña, *Pharmaceutics*, 2020, **12**, 371; (*b*) J. J. Rennick, A. P. R. Johnston and R. G. Parton, *Nat. Nanotechnol.*, 2021, **16**, 266–276.
18 B. Rathore, K. Sunwoo, P. Jangili, J. Kim, J. H. Kim, M. Huang, J. Xiong, A. Sharma, Z. Yang, J. Qu and J. S. Kim, *Biomaterials*, 2019, **211**, 25–47.
19 X. Ma, R. Xing, C. Yuan, K. Ogino and X. Yan, *View*, 2020, **1**, 20200020.
20 X. Chen, Z. Zhong, Z. Xu, L. Chen and Y. Wang, *Free Radical Res.*, 2010, **44**, 587–604.

